Buried Polar Interactions and Conformational Stability in the Simian Immunodeficiency Virus (SIV) gp41 Core[†]

Hong Ji, Clay Bracken, and Min Lu*

Department of Biochemistry, Weill Medical College of Cornell University, New York, New York 10021

Received August 13, 1999; Revised Manuscript Received October 18, 1999

ABSTRACT: For human (HIV) and simian (SIV) immunodeficiency viruses, the gp41 envelope protein undergoes a receptor-activated conformational change from a labile native structure to an energetically more stable fusogenic conformation, which then mediates viral-cell membrane fusion. The core structure of fusion-active gp41 is a six-helix bundle in which three antiparallel carboxyl-terminal helices are packed against an amino-terminal trimeric coiled coil. Here we show that a recombinant model of the SIV gp41 core, designated N36(L6)C34, forms an α-helical trimer that exhibits a cooperative two-state folding−unfolding transition. We investigate the importance of buried polar interactions in determining the overall fold of the gp41 core. We have replaced each of four polar amino acids at the heptad *a* and *d* positions of the coiled coil in N36(L6)C34 with a representative hydrophobic amino acid, isoleucine. The Q565I, T582I, and T586I variants form six-helix bundle structures that are significantly more stable than that of the wild-type peptide, whereas the Q575I variant misfolds into an insoluble aggregate under physiological conditions. Thus, the buried polar residues within the amino-terminal heptad repeat are important determinants of the structural specificity and stability of the gp41 core. We suggest that these conserved buried polar interactions play a role in governing the conformational state of the gp41 molecule.

For human (HIV)[1] and simian (SIV) immunodeficiency viruses, the envelope glycoprotein consists of a complex of the surface subunit gp120 and the transmembrane subunit gp41 (reviewed in refs *1*, *2*). gp120 recognizes the target cell by binding to both CD4 and particular chemokine receptors (*3*, *4*). gp41 then mediates fusion of the viral and cellular membranes, leading to release of viral genetic material into the cell. The structure and mechanism of the gp41 molecule has been studied extensively (for a recent review, see ref *5*). Protein dissection studies revealed that two 4-3 hydrophobic (heptad) repeat regions within the gp41 ectodomain form a stable helical trimer of antiparallel heterodimers (*6*−*8*; see Figure 1). X-ray crystallographic and NMR analyses confirmed that this soluble gp41 core folds into a six-helix bundle (*9*−*13*). The N (amino)-terminal helices form a central, trimeric coiled-coil, while the C (carboxyl)-terminal helices pack in an antiparallel orientation into hydrophobic grooves on the surface of this coiled-coil trimer. Recent data indicate that this six-helix structure represents the fusion-active conformation of gp41 and plays a direct role in membrane fusion (*6*, *9*−*11*, *14*, *15*).

Considerable evidence now implies that there are native (nonfusogenic) and fusion-active (fusogenic) states of viral membrane fusion proteins. The hemagglutinin (HA) protein of influenza virus, for example, undergoes a complex structural changes from the native to the fusogenic conformation when exposed to the acidic environment of the cellular endosome (*16*−*19*). This structural dimorphism is the basis for conformational changes that are crucial for activation of membrane fusion. Moreover, the HA protein in the native state is thought to be metastable and thus has the potential to transform to the energetically more stable fusogenic conformation (*18*, *20*, *21*). According to this view, membrane fusion is regulated by the conformational stability of viral fusion proteins.

The gp41 envelope protein is also thought to adopt two different tertiary structures (reviewed in refs *2*, *5*, *22*). The recently identified six-helix bundle structure corresponds to the core structure of fusion-active gp41 (*14*). In addition, synthetic peptides that make up this core complex are potent inhibitors of HIV-1 infection and syncytium formation (*6*, *23*−*25*). A large number of studies indicate that these peptides bind to gp41 and block transition to its fusogenic state through a dominant-negative mechanism (*6*, *26*−*33*). The structural and biophysical characteristics of the gp41 core and experiments on the inhibition of HIV-1 infection by gp41 peptides have led to the proposal that formation of the six-helix bundle brings the viral and cellular membranes into close proximity and thus overcomes the energy barrier for membrane fusion (*10*, *30*, *34*). Thus, the conformational specificity and stability of the six-helix bundle appear to be critical for addressing essential mechanistic questions about the gp41-mediated membrane fusion reaction.

[†] This work was supported by National Institutes of Health Grant AI42382 and by the New York City Council Speaker's Fund for Biomedical Research.

* To whom correspondence should be addressed. Mailing address: Department of Biochemistry, Weill Medical College of Cornell University, 1300 York Ave., New York, NY 10021. Telephone: 212-746-6562. Fax: 212-746−8875. E-mail: mlu@mail.med.cornell.edu.

[1] Abbreviations: HIV-1, human immunodeficiency virus type 1; SIV, simian immunodeficiency virus; PCR, polymerase chain reaction; IPTG, isopropylthio-β-D-galactoside; GdmCl, guanidinium hydrochloride; $[\theta]_{222}$, molar ellipticity at 222 nm; CD, circular dichroism; HPLC, high-performance liquid chromatography; T_m, midpoint of thermal denaturation; NMR, nuclear magnetic resonance; PBS, neutral pH phosphate-buffered saline; DSS, 3-(trimethylsilyl)-1-propanesulfonic acid.

10.1021/bi991893e CCC: $19.00 © 2000 American Chemical Society
Published on Web 01/06/2000

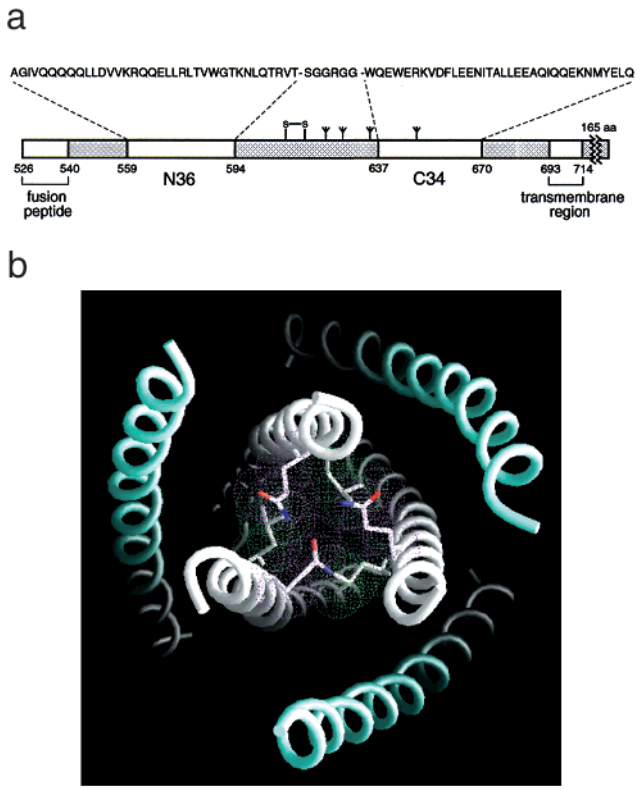

FIGURE 1: Core structure of SIV gp41. (A) Schematic representation of the SIV gp41 ectodomain. The important functional features of the gp41 ectodomain and the sequences of the N36 and C34 segments are shown. Recombinant N36(L6)C34 model consists of N36 and C34 plus a linker of six hydrophilic residues. The disulfide bond and four potential N-glycosylation sites are depicted. The residues are numbered according to their position in SIV gp160. (B) Axial view of the N36 and C34 complex from the NH_2 terminus looking down the 3-fold axis of the trimer (13). The N36 helices are colored white, whereas the C34 helices are blue. The van der Waals surfaces are colored purple for residues at the *a* positions and green for residues at the *d* positions of the interior N36 coiled-coil. Figure was created by using the program GRASP (*72*).

The N-terminal heptad-repeat sequence of gp41 is one of the most highly conserved regions within the immunodeficiency virus envelope glycoproteins (*35*−*37*). While the genetic evidence is compelling that this coiled-coil motif is held in the noncoiled-coil conformation in the native state (*38*−*41*), it forms a trimeric coiled-coil in the fusogenic state (*6*−*13*, *42*). Moreover, the folding and stability of the gp41 ectodomain core bearing mutations in this region correlate with severity of the in vivo phenotypes observed in cells expressing the mutant HIV-1 envelope glycoproteins (*15*, *38*). Taken together, these results have been interpreted to indicate that formation of the N-terminal coiled-coil underlies the mechanism of the gp41 conformational change (*15*, *26*, *41*). Therefore, it is of fundamental importance to define the determinants of structure and stability in this coiled-coil motif.

In our current study, we use the six-helix bundle formed by the SIV N36 and C34 peptides as a model system to investigate the role of buried polar interactions in determining the overall structure and thermodynamic stability of the gp41 core. The recombinant N36(L6)C34 peptide folds into a stable, α-helical trimer with an apparent $\Delta G°$ of −17.9 kcal mol^{-1}, evaluated from urea-denaturation experiments. We have substituted each of four polar residues in the hydrophobic interface of the N36 coiled coil in N36(L6)C34 with the hydrophobic amino acid isoleucine that can occupy both the *a* and *d* positions of a trimeric coiled coil (*43*). The Q575I mutant forms an insoluble aggregate under physiological conditions. In contrast, the Q565I, T582I, and T586I mutants fold into a trimeric, α-helical structure, and the stabilities of the folded mutants are significantly higher than that of the wild-type molecule. These results suggest that, whereas the Gln 575 side chain imparts specificity for formation of the six-helix bundle structure, the Gln 565, Thr 582, and Thr 586 residues contribute unfavorably to its thermodynamic stability. We suggest that these conserved polar interactions may play a role in controlling the gp41 conformational switch for activation of membrane fusion.

MATERIALS AND METHODS

Cloning and Mutagenesis. Plasmid pSIV38−149 (ref *7*) was used as a template to amplify the gene encoding for residues 563−670 from SIVmac239 by a polymerase chain reaction (PCR), with primers encoding a 5′ *Nde*I site and a 3′ *Bam*HI site as well as codons for amino-terminal Met-Ala-Gly-Ile-Val residues. The amplified 350 bp fragment was subsequently cloned into the *Nde*I and *Bam*HI sites of a phagemid-T7 expression vector, pAED4, to yield pSIVegp41. Plasmid pN36/C34, encoding the N36(L6)C34 model, was derived from pSIVegp41 by the insertion of the appropriate DNA sequences encoding the linker residues Ser-Gly-Gly-Arg-Gly-Gly between the C terminus of N36 and the N terminus of C34. Mutations were introduced into the N36(L6)C34 model by single-stranded mutagenesis (*44*) and verified by DNA sequencing. Standard recombinant DNA techniques were used (*45*).

Protein Production and Purification. All recombinant proteins were expressed in *Escherichia coli* BL21(DE3)/pLysS using the T7 expression system (*46*). Cells, freshly transformed with an appropriate plasmid, were grown to late log phase. Protein expression was induced by addition of 0.5 mM isopropylthio-β-D-galactoside (IPTG). After growth for another 3 h at 37 °C, the bacteria were harvested by centrifugation, and the cells were lysed by glacial acetic acid as described previously (*8*). Proteins were purified from the soluble fraction to homogeneity by reverse-phase high-performance liquid chromatography (HPLC), using a Vydac C-18 preparative column and a linear gradient of acetonitrile containing 0.1% trifluoroacetic acid. Uniformly ^{15}N-labeled protein samples were obtained by growing the bacteria in M9 minimal medium using $^{15}NH_4Cl$ as the sole nitrogen source. Protein identity was confirmed by mass spectrometry. Protein concentrations were determined by absorbance at 280 nm in 6 M guanidinium hydrochloride (GdmCl) using a calculated extinction coefficient (*47*).

Circular Dichroism Spectroscopy. CD spectra were acquired at a peptide concentration of 10 μM in neutral pH phosphate-buffered saline (PBS) [50 mM sodium phosphate, and 150 mM NaCl, adjusted to pH 7.0] with an Aviv 62 DS spectrometer. The wavelength dependence of molar ellipticity, [θ], was monitored as the average of five scans, using a five-second integration time at 1.0 nm wavelength increments. Spectra were baseline-corrected against the cuvette with buffer alone. Helix content was estimated from the CD signal by dividing the mean residue ellipticity at 222 nm by

the value expected for 100% helix formation by helices of comparable size, −33 000 deg.cm^2 dmol^{-1} (*48*). Thermal stability was determined by monitoring the change in CD signal at 222 nm as a function of temperature. Thermal melts were performed at two-degree intervals with a two-minute equilibration at the desired temperature, and an integration time of 30 s. Reversibility was checked by repeated scans. All melts were reversible, with superimposable folding and unfolding curves and >90% of the signal regained upon cooling. The midpoint of the thermal unfolding transition (melting temperature, T_m) was determined from the maximum of the first derivative, with respect to the reciprocal of the temperature, of the $[\theta]_{222}$ values (*49*). The error in estimation of T_m is ±1 °C. The relation $1/T_m = [2R(\ln C_T - \ln 6) + \Delta S^\circ]/\Delta H^\circ$ was used for the transition from a trimeric complex to three monomers (*50*). Urea-unfolding transition curves were measured in PBS (pH 7.0) by monitoring $[\theta]_{222}$ as a function of urea concentration. Samples were thermostated at 4 °C with a built-in temperature controller. A two-state unfolding model, with a linear dependence of ΔG on urea concentration (*51*), was fitted to the denaturation data using a fitting function developed by Backmann et al. (*52*) that describes the urea dependence of the CD signal for a monomer−trimer equilibrium. ΔG° represents the estimated standard free-energy difference (folded minus unfolded) in water between the folded and unfolded protein at 25 °C; *m* represents the first derivative of the free energy difference with respect to the concentration of urea.

Equilibrium Ultracentrifugation. Sedimentation equilibrium analysis was performed on a Beckman XL-A analytical ultracentrifuge. Protein solutions were dialyzed overnight against PBS, loaded at initial concentrations of 10, 30, and 100 μM, and analyzed at rotor speeds of 20 and 23 krpm at 20 °C. Data sets were fitted to a single-species model. Protein partial specific volume and solvent density were calculated with constants from Laue et al. (*53*). Molecular weights were all within 10% of those calculated for an ideal trimer.

NMR Spectroscopy. NMR samples were prepared by dissolving lyophilized peptide in 50 mM deuterated sodium formate (pH 4.0) and 1.9 or 3.6 M urea to give a peptide concentration of ~200 μM in 90% H_2O/10% D_2O solution. All spectra were acquired on a Varian INOVA AS600 spectrometer equipped with an 8 mm triple-resonance *Z*-axis gradient probe. Heteronuclear ^{15}N-correlation experiments were performed at 25, 44, and 63 °C, with spectral widths of 2200 and 8000 Hz in the indirect and acquisition dimensions, respectively. The temperature was calibrated using a 100% ethylene glycol sample, with calibration curves supplied by Varian Inc. (Palo Alto, CA). Two-dimensional (2D) ^{15}N-heteronuclear correlation spectra were collected with spectral widths of 2000 and 10000 Hz in the ^{15}N- and ^{1}H-dimensions, respectively. The proton carrier frequency was set to that of the water resonance and the ^{15}N carrier frequency was set to 118.24 ppm at 24.9 °C, 118.04 ppm at 43.8 °C, and 117.87 ppm at 62.7 °C. The ^{1}H-chemical shift was set using the H_2O chemical shift measured relative to DSS; the indirect ^{15}N-dimension was indirectly referenced as described by Live et al. (*54*), using the referencing ratio prescribed by Wishart et al. (*55*). All NMR spectra were processed and analyzed by using NMRPipe (*56*).

RESULTS

A Recombinant Model for the SIV gp41 Core. Previous studies showed that the overall architecture of the HIV-1 and SIV gp41 ectodomain cores is a six-helix bundle, in which three N-terminal peptides form an interior coiled coil, while three C-terminal peptides form outer helices that pack against the surface of the coiled coil in an antiparallel orientation (*6*−*13*; see Figure 1). To facilitate further studies, we designed and constructed a recombinant model of the SIV gp41 ectodomain core in which the N36 and C34 segments are connected by a six-residue hydrophilic linker in place of the disulfide-bonded loop region (Figure 1a). This SIV gp41 core model, designated N36(L6)C34, was produced by bacterial expression and purified by reverse-phase HPLC (see Materials and Methods).

The circular dichroism (CD) spectra of N36(L6)C34 are typical of an α-helical conformation, displaying minima at 208 and 222 nm and a maximum at 190 nm (Figure 2a). In neutral pH phosphate-buffered saline (PBS) at 10 μM peptide concentration and 0 °C, the ellipticity at 222 nm (θ_{222}) is −32 300 deg cm^2 dmol^{-1}, which corresponds to ~100% helical content (*48*). The spectra of N36(L6)C34 at all temperatures are well-represented by the population-weighted superposition of the α-helix and random-coil conformations (Figure 2a). The CD spectra also show a well-defined isodichroic point at 205 nm, indicating a two-state helix-to-coil transition (Figure 2a). The slight shift of isodichroic point in the far-UV CD spectrum of N36(L6)C34 is observed in other helical proteins and model peptides that contain aromatic residues (reviewed in ref *57*). The thermally induced unfolding transition of N36(L6)C34, as monitored by CD at 222 nm, is cooperative and reversible. The midpoint temperatures of the unfolding transition (T_m's) are 57, 60, 69, and 71 °C for 5, 10, 25, and 50 μM, respectively (Figure 2b). This concentration-dependent stability in the micromolar concentration range indicates that N36(L6)C34 self-associates. Additionally, the plot of $\ln C_T$ against $1/T_m$ is linear (Figure 2b, insert), reinforcing the observation that the thermal denaturation process of N36(L6)C34 represents a two-state helix-coil equilibrium (*50*).

Analytical ultracentrifugation sedimentation was used to determine the oligomerization state of N36(L6)C34. Over a 10-fold range of peptide concentrations, the apparent molecular mass of N36(L6)C34 is 28.3 kDa (Figure 2c). This value is in good agreement with an expected molecular mass of 26.8 kDa for a trimer, indicating that N36(L6)C34 is trimeric in solution. Moreover, the linear extrapolation method was used to evaluate the free energy change (ΔG°) for the unfolding of the N36(L6)C34 trimer. The urea-denaturation curve of N36(L6)C34 in the limit of zero concentration of urea yields an apparent ΔG° of −17.9 kcal mol^{-1} (Figure 2d). It should be noted that the simple linear extrapolation fitting procedure tends to underestimate ΔG° (*51*); −17.9 kcal mol^{-1} is thus a lower bound. In addition, the experimentally determined dependence of free-energy on urea concentration (the *m* value) was 2.0 kcal mol^{-1} M^{-1}. This value, which is indicative of the amount of surface area exposed to solvent upon unfolding (*58*), is in very good agreement with the expected values for the calculated total buried surface area. These results indicate that the recombinant N36(L6)C34 model folds into a defined six-helix

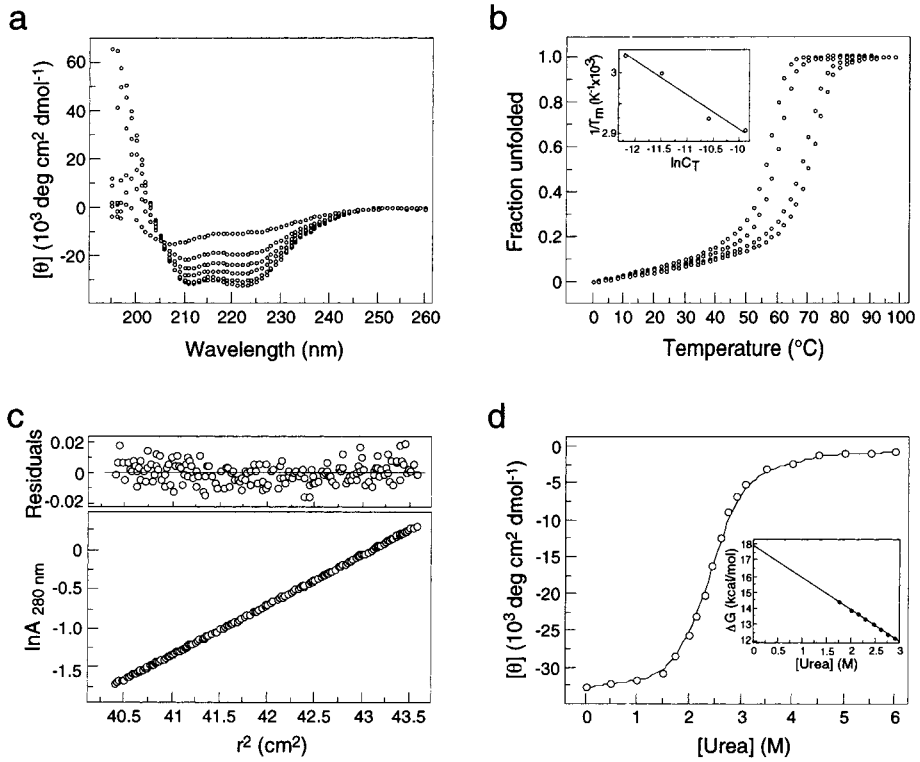

FIGURE 2: N36(L6)C34 forms a stable, helical trimer. (A) Circular dichroism (CD) spectra at (bottom to top curves) 0, 30, 50, 55, 60, and 65 °C in PBS (pH 7.0) at 10 μM peptide concentration. (B) Thermal melts monitored by CD at 222 nm at 5, 10, 25, and 50 μM (left to right curves) peptide concentrations in PBS (pH 7.0). The increase in the fraction of unfolded molecules is shown as a function of temperature. Insert shows the dependence of melting temperature on peptide concentration. (C) Analytical ultracentrifugation data (20 krpm) collected at 20 °C in PBS (pH 7.0) at ~30 μM peptide concentration. The natural logarithm of the absorbance at 280 nm is plotted against the square of the radial position. Deviations from the calculated values are plotted as residuals (Upper). (D) Urea-denaturation curve at 4 °C in PBS (pH 7.0) at 20 μM peptide concentration. The data were fit to a monomer-trimer equilibrium to yield an apparent $\Delta G°$ (25 °C) of −17.9 kcal mol^{-1} (m = 2.0 kcal mol^{-1} M^{-1}). Insert shows the linear extrapolation of the $\Delta G°$ value determined in the transition region to the limit of zero concentration of urea.

a

	559 d a d a d a d a d a 594
SIVmac239	AGIVQQQQQLLDVVKRQQELLRLTVWGTKNLQTRVT
HIV-1(A)	s.....sn..raiea.ghl.k.....i.q..a..l
HIV-1(B)	s.....nn..raiea..hl.q.....i.q..a.il
HIV-1(C)	s.....sn..raiea..hlmq.....i.q.....l
HIV-1(D)	s.....nn..raiea..hl.q.....i.q..a..l
HIV-1(E)	s.....sn..raiea..hl.q.....i.q..a..l
HIV-1(F)	s.....nn..raiea..hl.q.....i.q..a..l

b

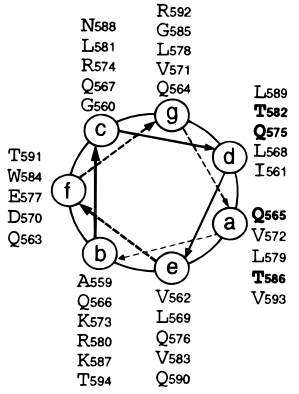

FIGURE 3: Buried polar residues within the N-terminal heptad-repeat region of gp41. (A) The N36 sequence of the SIVmac239 strain and the consensus N36 sequences of the HIV-1 strain classes. The heptad *a* and *d* positions are marked above the SIVmac239 sequence. The residues are numbered according to their position in SIV gp160. (B) Helical wheel projection of the N36 coiled-coil sequence of the SIVmac239 strain. The view is from the NH_2 terminus. Polar residues at the *a* and *d* positions are indicated by bold type.

bundle conformation that is well-suited for the thermodynamic analysis of the gp41 core and its mutants.

Hydrophobic Core Mutants of N36(L6)C34. The SIV N36 coiled-coil sequence contains four polar residues (Gln 565, Gln 575, Thr 582, and Thr 586) at the heptad *a* and *d* positions (Figure 3b). In the crystal structure of the N36 and C34 complex, these polar residues form a number of hydrogen bonds and salt bridges in an otherwise hydrophobic interface between the helices (*13*). Three of these polar residues are identical between SIV and HIV-1, whereas the analogous Thr 586 residue in HIV-1 strain classes is isoleucine (Figure 3a). Together, these buried polar interactions are likely to be critical for maintaining the six-helix bundle structure of the gp41 core. To directly test this notion, we replaced the four buried polar amino acids in N36(L6)C34 with the hydrophobic amino acid, isoleucine, individually and simultaneously. Isoleucine was selected because trimeric coiled coils tend to have β-branched residues (e.g., isoleucine) at both the *a* and *d* positions (*43*). The mutant N36(L6)C34 molecules were named by their positions

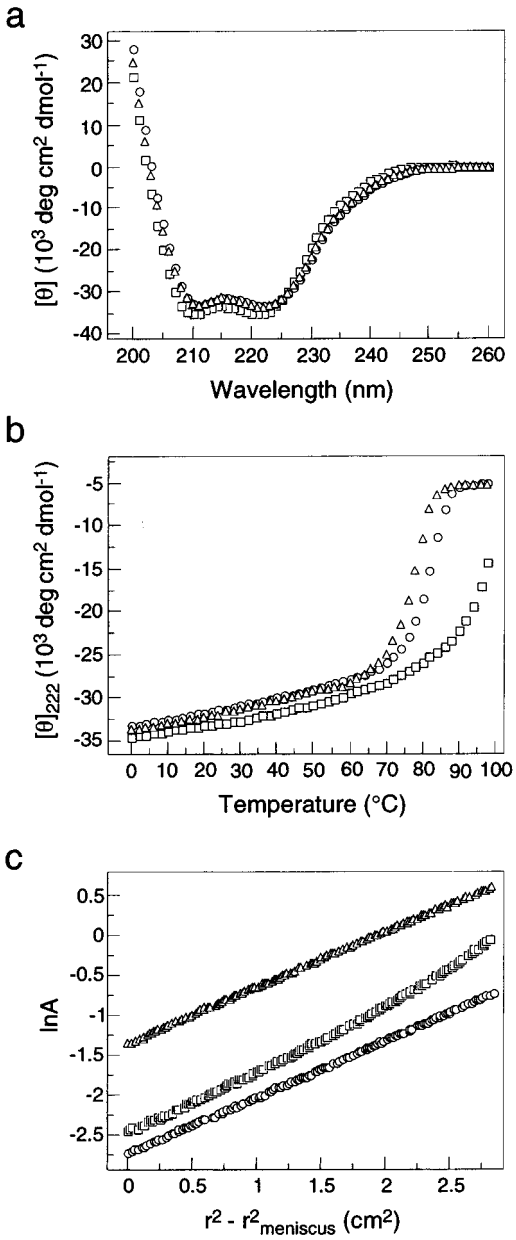

FIGURE 4: Influence of Thr 582 and Thr 586 on the thermal stability of N36(L6)C34. (A) CD spectra of T582I (triangles), T586I (circles), and T582I/T586I (squares) at 0 °C in PBS (pH 7.0) at 10 μM peptide concentration. (B) Thermal melts of T582I (triangles), T586I (circles), and T582I/T586I (squares) monitored by CD at 222 nm in PBS (pH 7.0) at 10 μM peptide concentration. (C) Analytical ultracentrifugation data (20 krpm) collected at 20 °C in PBS (pH 7.0) for T582I (~100 μM) (triangles), T586I (~10 μM) (circles), and T582I/T586I (30 μM) (squares).

of the substitution. All of these mutants were expressed in *E. coli* at high levels (~70 mg of protein per liter of culture).

The T582I and T586I Variants. The CD spectra of the T582I and T586I mutant peptides demonstrate that they are fully folded and exhibit cooperative and reversible melts (Figure 4a,b; Table 1). At 10 μM peptide concentration in PBS (pH 7.0), the T_m's of T582I and T586I are 77 and 81 °C, respectively (Figure 4b; Table 1). The increase in thermal stability, ΔT_m, between the wild-type and mutant peptides are 17 and 21 °C for T582I and T586I, respectively. Sedimentation equilibrium measurements indicate that both T582I and T586I form clean trimers (Figure 4c; Table 1). Thus, the Thr to Ile variants form extremely stable six-helix bundle structures. Moreover, T582I has an apparent $\Delta G°$ (25 °C) determined by urea denaturation of −19.4 kcal mol^{-1} (Table 1), whereas accurate determination of the ΔG value for T586I by urea unfolding experiments is complicated by difficulties establishing an unfolded baseline. The T582I mutant peptide is 1.5 kcal mol^{-1} more stable than the wild-type molecule (Table 1). The greater stabilizing effects observed for the isoleucine substitutions indicate that the buried Thr 582 and Thr 586 residues in the N-terminal coiled coil destabilize the gp41 core structure. By extension, these buried polar interactions appear to play a role in determining the thermodynamic stability of fusion-active gp41.

Table 1: Core Mutants of N36(L6)C34 Form Stable Six-helix Structures

core model	$-[\theta]_{222}$[a] (deg cm^2 dmol^{-1})	T_m[a] (°C)	T_m^{GdmCl}[c] (°C)	$\Delta G°$[d] (kcal mol^{-1})	molecular mass (kDa)
N36(L6)C34	32 300	60	<0	−17.9 ± 0.3	28.3
T582I	33 600	77	54	−19.4 ± 0.4	29.1
T586I	33 300	81	60		29.4
T582I/T586I	35 000	>96	83		32.9
Q565I	34 300	75	51	−18.9 ± 0.3	28.5
Q575I	34 400[b]		47		29.0

[a] All scans and melts were performed at 10 μM peptide concentration. [b] $[\theta]_{222}$ was measured in 1.5 M GdmCl. [c] T_m^{GdmCl} denotes the melting temperature in 1.5 M GdmCl. [d] The values of $\Delta G°$ are calculated by the method of Backmann et al. (*52*) at 25 °C. Errors are given as standard deviations.

The T582I/T586I Variant. To determine whether both Thr 582 and Thr 586 are necessary for adopting the six-helix bundle fold, we studied the double mutant T582I/T586I peptide. On the basis of CD measurements at 10 μM peptide concentration in PBS (pH 7.0), T582I/T586I is fully helical and has a thermal stability that exceeds 96 °C (Figure 4a,b; Table 1). In the presence of the denaturant guanidinium hydrochloride (GdmCl) at 1.5 M concentration, T582I/T586I melts cooperatively with an apparent T_m of 83 °C, compared with apparent T_m's of 54 and 60 °C for T582I and T586I, respectively, under the same conditions (Table 1). Thus, the stabilizing effects of the two single mutations appear to be additive. Moreover, the double mutant peptide is also trimeric in PBS (pH 7.0) at 20 °C, and the apparent molecular mass is concentration-independent between 10 and 100 μM (Figure 4c; Table 1). However, a systematic trend is observed in the residuals between the data and the linear fit (Figure 4c), suggesting that the T582I/T586I peptide is prone to aggregation.

NMR spectroscopy was used to further characterize the solution properties of T582I/T586I in 50 mM sodium formate (pH 4.0) and 1.9 M urea. Under these conditions, T582I/T586I is soluble up to peptide concentrations of ~200 μM. Figure 5 shows the two-dimensional ^{1}H-^{15}N correlation spectra of N36(L6)C34 (wild-type) at 25 °C and T582I/T586I at 25, 44, and 63 °C. In general, the wild-type and double mutant peptide spectra at 25 °C show a similar degree of chemical shift dispersion in the amide resonances of peptide backbone and the glutamine and asparagine side chains (Figure 5a,b). However, the spectrum of the double mutant at 25 °C displays significantly greater chemical shift degeneracy in both the ^{1}H- and ^{15}N-dimensions, and large line-width and intensity variations between resonances (Figure 5b), suggesting conformational heterogeneity. This

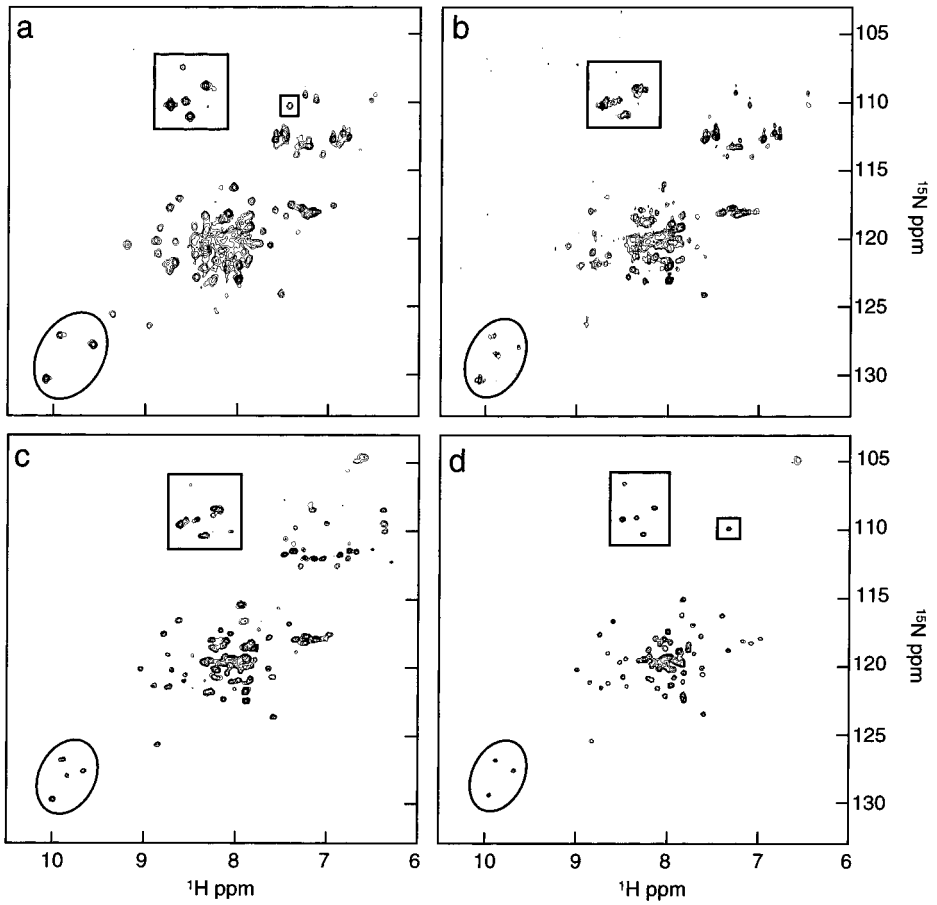

FIGURE 5: The ^{1}H-^{15}N heteronuclear single quantum coherence correlation spectra of N36(L6)C34 at 25 °C (A) and T582I/T586I at 25 °C (B), 44 °C (C), and 63 °C (D) in 50 mM deuterated sodium formate (pH 4.0) and 1.9 M urea at ~200 μM peptide concentration. The resonances for the glycine amides and tryptophan indole protons are boxed and circled, respectively.

is clearly seen in less congested regions corresponding to the glycine amides (boxed in Figure 5b) and three tryptophan indole protons (circled in Figure 5b). The multiplicity in resonances of T582I/T586I at 25 °C indicates that a variety of distinct chemical environments are present in solution on a time scale of milliseconds or greater.

Upon heating, the apparent chemical shift heterogeneity and line-broadening in the ^{1}H-^{15}N correlation spectra of the double mutant is gradually eliminated (Figure 5c,d). At 63 °C, the backbone amide region contains 66 distinct cross-peaks out of 75 peaks expected for the backbone amide in T582I/T586I, consistent with a single defined conformation or rapid conformational averaging. Remarkably, the chemical shift dispersion in the double mutant at 63 °C (Figure 5d) is comparable to that seen in the wild-type molecule at 25 °C (Figure 5a); this is especially evident in the patterns of resonances in regions typically occupied by the glycine amides (boxed) and tryptophan indole protons (circled) (Figure 5a,d). Thus, heat can serve to destabilize alternative conformers of T582I/T586I, thereby populating the most stable six-helix bundle structure of the peptide. Collectively, these results indicate that the buried Thr 582 and Thr 586 residues within the N-terminal heptad repeat are required for the correct folding of the gp41 ectodomain core.

The Q565I Variant. The CD spectrum of the Q565I variant indicates that the folded mutant peptide contains ~100% α-helical structure, which sedimentation equilibrium indicates is a clean trimer (observed molecular mass 28.5 kDa; expected for a trimer 26.7 kDa) (Table 1). The T_m for the unfolding of Q565I is 75 °C in PBS (pH 7.0) at 10 μM peptide concentration, as compared with 60 °C for the wild-type peptide (Table 1). Linear extrapolation of the urea denaturation of the Q652I trimer to 0 M urea yields an apparent $\Delta G°$ (25 °C) value of −18.9 kcal mol^{-1} (Table 1). The nonpolar Gln 565 to Ile mutation stabilizes the N36(L6)C34 trimer by 1.0 kcal mol^{-1}. These results consistent with the observation that buried polar residues in coiled coils are generally destabilizing (e.g., ref *59*). Thus, the conserved Gln 565 residue contributes unfavorably to the conformational stability of the gp41 core.

The Q575I Variant. The Q575I mutant peptide is not soluble in water and forms an insoluble aggregate in PBS (pH 7.0), presumably due to misfolding of the molecule. In the presence of 1.5 M GdmCl, Q575I becomes soluble up to concentrations of ~60 μM in PBS (pH 7.0). Under these conditions, Q575I folds into a fully helical conformation and exhibits a thermally induced unfolding transition, with an apparent T_m of 47 °C at 10 μM peptide concentration (Figure 6b; Table 1). Over a 5-fold range of peptide concentration (10, 25, and 50 μM), the averaged experimental molecular mass of Q575I is 29.0 kDa, as determined by sedimentation equilibrium (Figure 6c; Table 1). This value is in good agreement with the calculated molecular mass for trimer (26.7 kDa), indicating that Q575I is trimeric in the presence of 1.5 M GdmCl. Our results suggest that Q575I tends to exist in alternate/misfolded conformations, culminating in the formation of a protein aggregate, under physiological

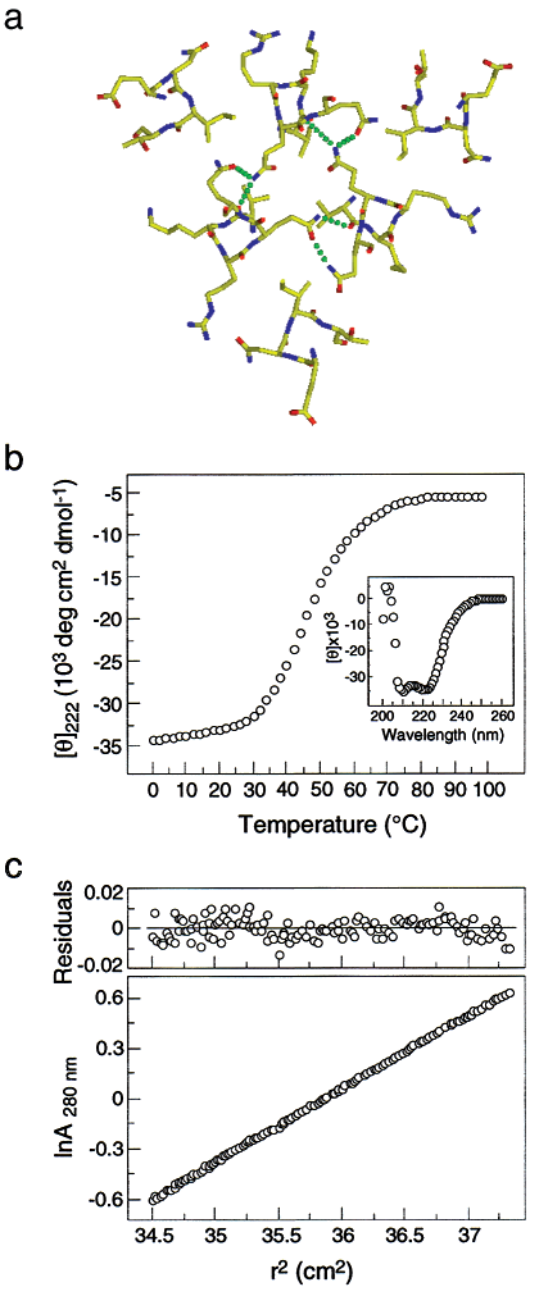

FIGURE 6: Q575I forms a helical trimer in the presence of 1.5 M GdmCl. (A) Helix packing around Gln 575 in the crystal structure of the N36−C34 complex (*13*). Hydrogen bonds are shown in green as broken lines. Figure was generated by using the program SETOR (*73*). (B) Thermal melt of Q575I monitored by CD at 222 nm in PBS (pH 7.0) at 10 μM peptide concentration in the presence of 1.5 M GdmCl. Insert shows the CD spectrum of Q575I at 0 °C. (C) Analytical ultracentrifugation data (20 krpm) collected at 20 °C in PBS (pH 7.0) at ~25 μM peptide concentration in the presence of 1.5 M GdmCl. The natural logarithm of the absorbance at 280 nm is plotted against the square of the radial position. Deviations from the calculated values are plotted as residuals (Upper).

conditions and that the denaturant GdmCl can destabilize the misfolded conformers and shift the equilibrium in favor of the native-like six-helix bundle conformation. In addition, when Gln 575 is replaced by asparagine, the N36(L6)C34 mutant peptide forms an insoluble aggregate in PBS (pH 7.0). Because asparagine and glutamine differ by a single methylene group, the packing geometries of the Gln 575 side chain appear to play a key role in specifying the gp41 core structure.

The Q565I/T582I/T586I Variant. To examine whether the Gln 575 side chain is sufficient for imparting specificity for the six-helix complex formation, we substituted Gln 565 with isoleucine in the T582/*T*586 double mutant to produce a triple mutant (Q565I/T582I/T586I). This triple mutant peptide is insoluble in water. In the presence of 3 M GdmCl, the triple mutant peptide forms a fully helical structure, which melts cooperatively and reversibly with a T_m of 84 °C in PBS (pH 7.0) at 10 μM peptide concentration (Figure 7a). Under these conditions, this peptide sediments as a clean trimer by sedimentation equilibrium (Figure 7b). Moreover, the ^{1}H-^{15}N heteronuclear NMR spectrum of Q565I/T582I/T586I in 50 mM sodium formate (pH 4.0) and 3.6 M urea at 25 °C shows significant chemical shift heterogeneity in amide resonances, suggesting the existence of multiple conformers in solution (Figure 7c,d). However, the spectrum collected at 45 °C exhibits better-resolved resonances for the amide groups in the peptide (Figure 7c,d). These results indicate that Q565I/T582I/T586I fails to form a six-helix bundle conformation with the high level of structural uniqueness observed in the wild-type peptide.

DISCUSSION

Contribution of Buried Polar Interactions to the gp41 Core Folding and Stability. While recent structural and biophysical studies of the gp41 ectodomain core provide detailed information about the fusogenic conformation of the molecule, the factors that determine the overall structure and stability of this core are not well-understood. Our results show that the recombinant SIV N36(L6)C34 model forms a six-helix bundle that undergoes a two-state unfolding transition by heat or upon addition of urea. Our results also show that the gp41 core domain formed by N36(L6)C34 is of high stability, with a $\Delta G°$ value of −17.9 kcal mol^{-1} at 25 °C, as determined by urea denaturation. For comparison, the folded state of most proteins is stabilized by −5 to −15 kcal mol^{-1} at 25 °C, relative to the unfolded state (*60*). In addition, NMR studies indicate that N36(L6)C34 folds into a single, discrete conformation under physiological conditions. The N36(L6)C34 peptide constitutes a tractable model system to understand the structural uniqueness of the gp41 core and measure the conformational stability of this core and its mutants.

Globular proteins exhibit a segregation of hydrophobic and polar residues, with hydrophobic residues in the protein interior and polar residues generally on the protein surface, suggesting that the drive to bury hydrophobic residues can specify unique tertiary structures (*61*). Recent evidence suggests that the burial of a polar residue in the hydrophobic interior of a protein favors structural uniqueness and specificity but is destabilizing relative to substitution by a hydrophobic isostere (e.g., ref *59*). Despite a simple hydrophobic-polar residue pattern, coiled-coil sequences can adopt parallel or antiparallel dimeric as well as trimeric and tetrameric conformations (reviewed in ref *62*). Specific packing interactions are required to guide a coiled-coil sequence to a single structure (*59*, *63*). In particular, buried polar interactions and the geometric properties of buried side chains in coiled coils are essential determinants of the overall structure (*59*, *63*).

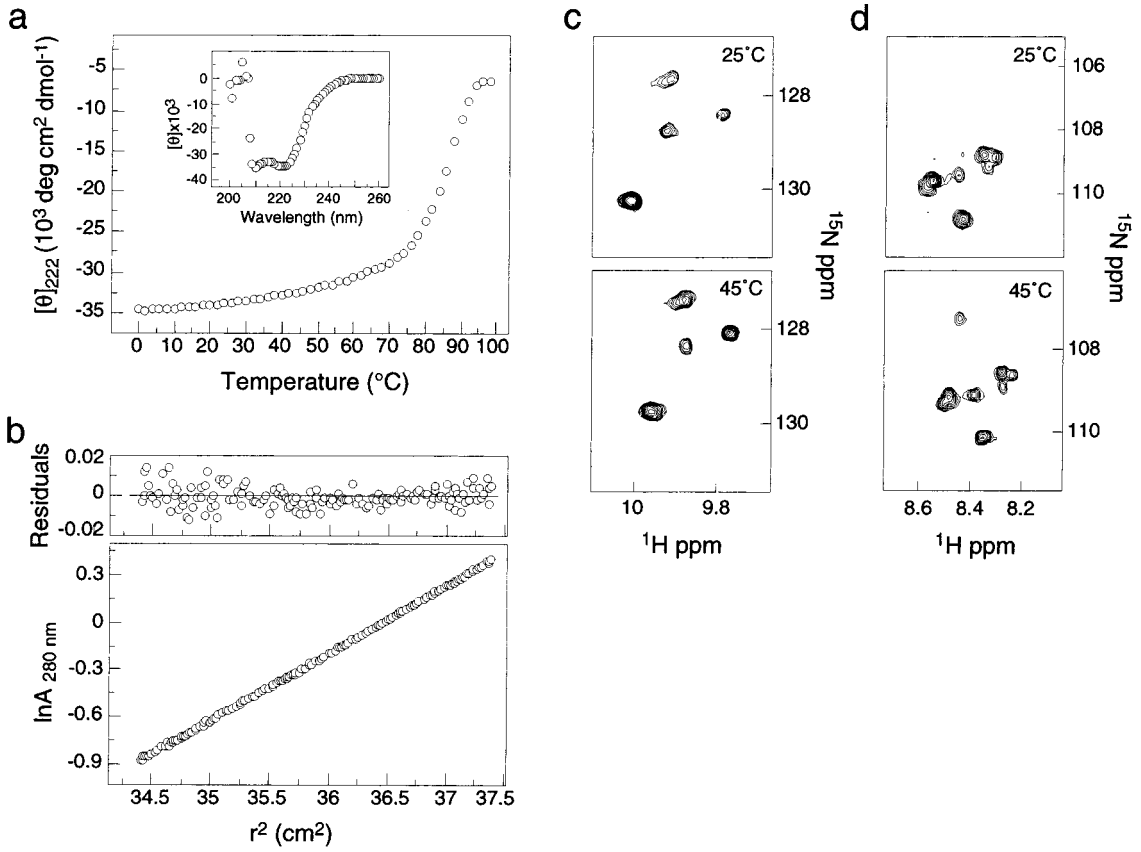

FIGURE 7: The T582I/T586I/Q565I triple mutant forms a stable helical trimer in the presence of 3 M GdmCl. (A) Thermal melt monitored by CD at 222 nm in PBS (pH 7.0) at 10 μM peptide concentration in the presence of 3 M GdmCl. Insert shows the CD spectrum at 0 °C. (B) Analytical ultracentrifugation data (20 krpm) collected at 20 °C in PBS (pH 7.0) at ~30 μM peptide concentration in the presence of 3 M GdmCl. The natural logarithm of the absorbance at 280 nm is plotted against the square of the radial position. Deviations from the calculated values are plotted as residuals (Upper). (C) ^{1}H-^{15}N heteronuclear single quantum coherence correlation spectra showing resonances expected for three tryptophan indole protons at 25 and 45 °C in 50 mM deuterated sodium formate (pH 4.0) and 3.6 M urea at ~200 μM peptide concentration. (D) ^{1}H-^{15}N heteronuclear spectra showing five out of six cross-peaks expected for the glycine amides at 25 and 45 °C in 50 mM deuterated sodium formate (pH 4.0) and 3.6 M urea at ~200 μM peptide concentration.

Notably, there are four polar residues at the *a* and *d* heptad positions in the SIV N36 helix region (see Figure 3). X-ray crystallographic studies of the gp41 core demonstrate that these polar residues are involved in the formation of hydrogen bonds and salt bridges, which are distributed along the N36 helices and interdigitated with the hydrophobic contacts (*13*). The isoleucine replacements for the buried polar residues characterized here indicate that they are responsible for conferring structural selectivity and conformational stability on the gp41 core. Our results show that the Q565I, T582I, and T586I variants form well-structured six-helix bundles that are significantly more stable than that of the wild-type peptide. In contrast, the Q575I variant forms an insoluble aggregate under physiological conditions (i.e., PBS). In the case of Q575I, misfolding and aggregation could be due to a thermodynamic or kinetic barrier or both. Isoleucine at the 575 position of N36(L6)C34 may fail to produce a sufficient free energy difference between the six-helix bundle structure and all other conformers. Interestingly, we find that either heat or the denaturant GdmCl can promote the formation of a unique six-helix bundle conformation. We show that the T582I/T586I double mutant and the Q565I/T582I/T586I triple mutant form exceedingly stable six-helix structures at the expense of structural uniqueness. The NMR spectra of these mutant peptides at 25 °C display distinct spectral differences from the wild-type peptide, suggesting either the presence of aggregation or multiple conformational states. However, the spectral patterning of the double mutant at 63 °C bears greater similarity to that of the wild-type peptide at 25 °C. Our results are consistent with the notion that buried polar residues contribute to the structural uniqueness of a protein by destabilizing alternative non-native-like interactions. It is also possible that the folding kinetics of the hydrophobic core mutants of N36(L6)C34 may be slow and complex in comparison to the wild-type peptide. Previous studies have shown that addition of heat or high concentrations of urea increases the rate of protein folding to the final folded structure (e.g., ref *64*).

Implications for Viral Membrane Fusion. It is generally accepted that viral membrane fusion proteins can adopt two different conformations (i.e., native and fusogenic states). The low-pH-induced conformational change in the HA protein of influenza virus is understood in greater detail (*16*−*19*). Recent evidence shows that HA is most stable in its fusogenic state, while HA in its native state is metastable (*18*, *20*, *21*). The metastability model for membrane fusion activation postulates that the fusogenic conformation of HA is released by destabilization of the native structure (*21*). For HIV-1 and SIV, binding of gp120 to target cell receptors triggers the membrane fusion activity of gp41. This receptor-binding-promoted fusion activation is also thought to involve a conformational change in gp41 from a native to a fusogenic

state, although few details are understood (reviewed in refs *2*, *5*). Given that the six-helix bundle structure of the gp41 core is exceedingly stable to thermal denaturation and resembles the low-pH-induced conformation of the HA protein, it was suggested that this structure represents the fusogenic conformation of gp41 (*6*, *9*−*11*). This view has been confirmed by the finding that a monoclonal antibody recognizing the six-helix bundle binds to the surface of HIV-1 infected cells only after interaction of the gp120 and gp41 complex with the soluble CD4 receptor (*14*). The structure of gp41 in the native conformation is not known.

Formation of the N-terminal coiled-coil structure in gp41 is thought to play a dominant role in the conformational change in the gp120 and gp41 complex required for fusion activation (*15*, *26*, *33*, *41*). In the atomic structure of the gp41 ectodomain core, the N-terminal trimeric coiled coil is surrounded by three antiparallel C-terminal helices that are packed into hydrophobic grooves on the surface of the coiled-coil trimer (*9*−*13*). Mutagenesis studies indicate that mutations in this coiled-coil sequence abolish membrane fusion activity but have little effect on the native gp120−gp41 complex on the surface of the virion (*38*−*41*). A correlation is observed between mutational effects on the fusion activity of the HIV-1 envelope glycoprotein and the folding and stability of the HIV-1 gp41 core (*15*, *33*). These results can be reconciled by the suggestion that these mutations do not disrupt the native structure of gp41 but do inhibit its conformational change to the fusogenic state (*26*, *41*). According to this suggestion, the gp41 conformational change is driven by the formation of the N-terminal coiled-coil. Our results indicate that buried polar interactions within this coiled-coil motif can determine the folding and conformational stability of the gp41 core. One might envision that these highly conserved interactions may help tip the balance between the metastable native and most stable fusogenic states of gp41 by destabilizing the fusogenic structure, as opposed to stabilizing the labile native conformation.

While the envelope glycoproteins of HIV-1 and SIV share many common features, several differences have been observed between laboratory-adapted strains of HIV-1 and SIV. First, binding of soluble CD4 to some laboratory-adapted isolates of HIV-1 induces the dissociation (shedding) of gp120 from the transmembrane gp41 subunit (*65*, *66*). In contrast, efficient gp120 shedding in the case of SIV has not yet been demonstrated (*67*). Second, the gp120 and gp41 subunits associate more tightly in SIV than in HIV-1 (*68*, *69*). Finally, addition of low levels of soluble CD4 block HIV-1 infection of human T-cell lines but enhances infection of SIV and some primary isolates of HIV-1 (*65*, *70*, *71*). Interestingly, the gp41 core structure of HIV-1 is significantly more stable than that of SIV (melting temperature of 66 vs 40 °C) (*8*, *13*). Comparing HIV-1 and SIV, one nonconservative change exists at the *a* position of the N-terminal heptad-repeat region of gp41 (Thr 586 in SIV and Ile in the corresponding position of HIV-1). Our results indicate that this substitution can increase the thermal stability of the SIV gp41 core by 21 °C, suggesting that the buried Thr 586 side chain in the case of SIV destabilizes the six-helix bundle structure, relative to its HIV-1 counterpart. This destabilization effect could be related to phenotypic differences between HIV-1 and SIV. Given that the driving force for the gp41 conformational change is the formation of the N-terminal-coiled coil (*15*, *26*, *41*), it is possible that the polar atom of Thr 586 within the SIV coiled-coil may reduce the free energy difference between the native and fusogenic conformations, thereby stabilizing the native gp120−gp41 complex of SIV, relative to that of HIV-1. Further comparative studies on the structural and biophysical properties of the HIV-1 and SIV envelope glycoproteins will provide new insights into the mechanism of retroviral-induced membrane fusion.

REFERENCES

1. Hunter, E., and Swanstrom, R. (1990) *Curr. Top. Microbiol. Immunol. 157*, 187−253.
2. Moore, J. P., Jameson, B. A., Weiss, R. A., and Sattentau, Q. J. (1993) In *Viral Fusion Mechanisms* (Bentz, J., Ed.) pp 233−289, CRC Press, Boca Raton, FL.
3. Kwong, P. D., Wyatt, R., Robinson, J., Sweet, R. W., Sodroski, J., and Hendrickson, W. A. (1998) *Nature 393*, 648−659.
4. Rizzuto, C. D., Wyatt, R., Hernandez-Ramos, N., Sun, Y., Kwong, P. D., Hendrickson, W. A., and Sodroski, J. (1998) *Science 280*, 1949−1953.
5. Chan, D. C., and Kim, P. S. (1998) *Cell 93*, 681−684.
6. Lu, M., Blacklow, S. C., and Kim, P. S. (1995) *Nat. Struct. Biol. 2*, 1075−1082.
7. Blacklow, S. C., Lu, M., and Kim, P. S. (1995) *Biochemistry 34*, 14955−14962.
8. Lu, M., and Kim, P. S. (1997) *J. Biomol. Struct. Dyn. 15*, 465−471.
9. Chan, D. C., Fass, D., Berger, J. M., and Kim, P. S. (1997) *Cell 89*, 263−273.
10. Weissenhorn, W., Dessen, A., Harrison, S. C., Skehel, J. J., and Wiley, D. C. (1997) *Nature 387*, 426−430.
11. Tan, K., Liu, J., Wang, J., Shen, S., and Lu, M. (1997) *Proc. Natl. Acad. Sci. U.S.A. 94*, 12303−12308.
12. Caffrey, M., Cai, M., Kaufman, J., Stahl, S. J., Wingfield, P. T., Covell, D. G., Gronenborn, A. M., and Clore, G. M. (1998) *EMBO J. 17*, 4572−4584.
13. Malaskkevich, V. N., Chan, D. C., Chutkowski, C. T., and Kim, P. S. (1998) *Proc. Natl. Acad. Sci. U.S.A. 95*, 9134−9139.
14. Jiang, S, Lin, K, and Lu, M. (1998) *J. Virol. 72*, 10213−10217.
15. Lu, M., Ji, H., and Shen, S. (1999) *J. Virol. 73*, 4433−4438.
16. Wiley, D. C., and Skehel, J. J. (1987) *Annu. Rev. Biochem. 56*, 365−394.
17. Stegmann, T., and Helenius, A. (1993) in *Viral Fusion Mechanisms* (Bentz, J., Ed.) pp 233−289, CRC Press, Boca Raton, FL.
18. Carr, C. M., and Kim, P. S. (1993) *Cell 73*, 823−832.
19. Bullough, P. A., Hughson, F. M., Skehel, J. J., and Wiley, D. C. (1994) *Nature 371*, 37−43.
20. Chen, J., Wharton, S. A., Weissenhorn, W., Calder, L. J., Hughson, F. M., Skehel, J. J., and Wiley, D. C. (1995) *Proc. Natl. Acad. Sci. U.S.A. 92*, 12205−12209.
21. Carr, C. M., Chaudhry, C., and Kim, P. S. (1997) *Proc. Natl. Acad. Sci. U.S.A. 94*, 14306−14313.
22. Skehel, J. J., and Wiley, D. C. (1998) *Cell 95*, 871−874.
23. Wild, C. T., Oas, T., McDanal, C. B., Bolognesi, D., and Matthews, T. J. (1992) *Proc. Natl. Acad. Sci. U.S.A. 89*, 10537−10541.
24. Jiang, S., Lin, K., Strick, N., and Neurath, A. R. (1993) *Nature 365*, 113.
25. Wild, C. T., Shugars, D. C., Greenwell, T. K., McDanal, C. B., and Matthews, T. J. (1994) *Proc. Natl. Acad. Sci. U.S.A. 91*, 9770−9774.
26. Chen, C. H., Matthews, T. J., McDanal, C. B., Bolognesi, D. P., and Greenberg, M. L. (1995) *J. Virol. 69*, 3771−3777.
27. Wild, C. T., Greenwell, T., Shugars, D., Rimsky-Clarke, L., and Matthews, T. (1995) *AIDS Res. Hum. Retroviruses 11*, 323−325.
28. Judice, J. K., Tom, J. Y. K., Huang, W., Wrin, T., Vennari, J., Petropoulos, C. J., and McDowell, R. S. (1997) *Proc. Natl. Acad. Sci. U.S.A. 94*, 13426−13430.

29. Rimsky, L. T., Shugars, D. C., and Matthews, T. J. (1998) *J. Virol. 72*, 986−993.
30. Furuta, R. A., Wild, C. T., Weng, Y., and Weiss, C. D. (1998) *Nat. Struct. Biol. 5*, 276−279.
31. Munoz-Barroso, I., Durell, S., Sakaguchi, K., Appella, E., and Blumenthal, R. (1998) *J. Cell Biol. 140*, 315−323.
32. Chan, D. C., Chutkowski, C. T., and Kim, P. S. (1998) *Proc. Natl. Acad. Sci. U.S.A. 95*, 15613−15617.
33. Ji, H., Shu, W., Burling, F. T., Jiang, S., and Lu, M. (1999) *J. Virol. 73*, 8578−8586.
34. Hughson, F. M. (1997) *Curr. Biol. 7*, R565−R569.
35. Delwart, E. J., Mosialos, G., and Gilmore, T. (1990) *AIDS Res. Hum. Retroviruses 6*, 703−706.
36. Chambers, P., Pringle, C. R., and Easton, A. J. (1990) *J. Gen. Virol. 71*, 3075−3080.
37. Gallaher, W. R., Ball, J. M., Garry, R. F., Griffin, M. C., and Montelaro, R. C. (1989) *AIDS Res. Hum. Retroviruses 5*, 431−440.
38. Dubay, J. W., Roberts, S. J., Brody, B., and Hunter, E. (1992) *J. Virol. 66*, 4748−4756.
39. Cao, J., Bergeron, L., Helseth, E., Thali, M., Repke, H., and Sodroski, J. (1993) *J. Virol. 67*, 2747−2755.
40. Chen, S. S., Lee, C. N., Lee, W. R., McIntosh, K., and Lee, T. H. (1993) *J. Virol. 67*, 3615−3619.
41. Wild, C. T., Dubay, J. W., Greenwell, T. K., Baird, Jr. T., Oas, T. G., McDanal, C. B., Hunter, E., and Matthews, T. J. (1994) *Proc. Natl. Acad. Sci. U.S.A. 91*, 12676−12680.
42. Shu, W., Ji, H., and Lu, M. (1999) *Biochemistry 38*, 5378−5385.
43. Harbury, P. B., Kim, P. S., and Alber, T. (1994) *Nature 371*, 80−83.
44. Kunkel, T. A., Roberts, J. D., and Zakour, R. A. (1987) *Methods Enzymol. 154*, 367−382.
45. Sambrook, J., Fritsch, E. F., and Maniatis, T. (1989) *Molecular Cloning: A Laboratory Manual*. Cold Spring Harbor Laboratory Press, Cold Spring Harbor, NY.
46. Studier, F. W., Rosenberg, A. H., Dunn, J. J., and Dubendorff, J. W. (1990) *Methods Enzymol. 185*, 60−89.
47. Edelhoch, H. (1967) *Biochemistry 6*, 1948−1954.
48. Chen, Y.-H., Yang, J. T., and Chau, K. H. (1974) *Biochemistry 13*, 3350−3359.
49. Cantor, C., and Schimmel, P. (1980) *Biophysical Chemistry*, Freeman, New York.
50. Marky, L. A., and Bresslauer, K. J. (1987) *Biopolymers 26*, 1601−1620.
51. Santoro, M. M., and Bolen, D. W. (1988) *Biochemistry 27*, 8063−8068.
52. Backmann, J., Schafer, G., Wyns, L., and Bonisch, H. (1998) *J. Mol. Biol. 284*, 817−833.
53. Laue, T. M., Shah, B. D., Ridgeway, T. M., and Pelletier, S. L. (1992) in *Analytical Ultracentrifugation in Biochemistry and Polymer Science* (Harding, S. E., Rowe, A. J., and Horton, J. C., Eds.) pp 90−125, The Royal Society of Chemistry, Cambridge, U.K.
54. Live, D. H., Davis, D. G., Agosta, W. C., and Cowburn, D. (1984) *J. Am. Chem. Soc. 106*, 1939−1941.
55. Wishart, D. S., Bigam, C. G., Yao, J., Abildgaard, F., Dyson, H. J., Oldfield, E., Markley, J. L., and Sykes, B. D. (1995) *J. Biomol. NMR 6*, 135−140.
56. Delaglio, F., Grzesiek, S., Vuister, G., Zhu, G., Pfeifer, J., and Bax, A. (1995) *J. Biomol. NMR 6*, 227−293.
57. Kallenbach, N. R., Zhou, H. X., and Lyu, P. C. (1996) in *Circular Dichroism and the Conformational Analysis of Biomolecules* (Fasman, G. D., Ed.) pp 201−259, Plenum Press, New York.
58. Myers, J. K., Pace, C. N., and Scholtz, J. M. (1995) *Protein Sci. 4*, 2138−2148.
59. Harbury, P. B., Zhang, T., Kim, P. S., and Alber, T. (1993) *Science 262*, 1401−1407.
60. Privalov, P. L. (1979) *Adv. Protein Chem. 33*, 167−241.
61. Dill, K. A. (1990) *Biochemistry 29*, 7133−7155.
62. Betz, S. F., Bryson, J. W., and DeGrado, W. F. (1995) *Curr. Opin. Struct. Biol. 5*, 457−463.
63. Gonzalez, Jr. L., Woolfson, D. N., and Alber, T. (1996) *Nat. Struct. Biol. 3*, 1011−1018.
64. Weissman, J. S., and Kim, P. S. (1991) *Science 253*, 1386−1393.
65. Moore, J. P., McKeating, J. A., Weiss, R. A., and Sattentau, Q. J. (1990) *Science 250*, 1139−1142.
66. Hart, T. K., Kirsh, R., Ellens, H., Sweet, R. W., Lambert, D. M., Petteway, S. R., Jr., Leary, J., and Bugelski, P. J. (1991) *Proc. Natl. Acad. Sci. U.S.A.* 88, 2189−2193.
67. Allan, J. S. (1991) *Science 252*, 1322−1323.
68. Sattentau, Q. J., and Moore, J. P. (1993) *Philos. Trans. R. Soc. B 342*, 59−66.
69. Sattentau, Q. J., Moore, J. P., Vignaux, F., Traincard, F., and Poignard, P. (1993) *J. Virol. 67*, 7383−7393.
70. Allan, J. S., Strauss, J., and Buck, D. W. (1990) *Science 247*, 1084−1088.
71. Sullivan, N., Sun, Y., Li, J., Hofmann, W., and Sodroski, J. (1995) *J. Virol. 69*, 4413−4422.
72. Nicholls, A., Sharp. K. A., and Honig, B. (1991) *Proteins 11*, 281−296.
73. Evans, S. V. (1993) *J. Mol. Graphics 11*, 134−138.

BI991893E